HAL open science

Monitoring the aspect ratio distribution of colloidal gold nanoparticles under pulsed-laser exposure

Yehia Mansour, Yann Battie, Aotmane En Naciri, Nouari Chaoui

To cite this version:

Yehia Mansour, Yann Battie, Aotmane En Naciri, Nouari Chaoui. Monitoring the aspect ratio distribution of colloidal gold nanoparticles under pulsed-laser exposure. Optics Express, 2020, 28 (23), pp.34501-34515. 10.1364/OE.399831 . hal-02986667

HAL Id: hal-02986667

https://hal.science/hal-02986667v1

Submitted on 28 Jan 2022

HAL is a multi-disciplinary open access archive for the deposit and dissemination of scientific research documents, whether they are published or not. The documents may come from teaching and research institutions in France or abroad, or from public or private research centers.

L'archive ouverte pluridisciplinaire **HAL**, est destinée au dépôt et à la diffusion de documents scientifiques de niveau recherche, publiés ou non, émanant des établissements d'enseignement et de recherche français ou étrangers, des laboratoires publics ou privés.

Distributed under a Creative Commons Attribution 4.0 International License

Important Notice to Authors

Attached is a PDF proof of your forthcoming article in Optics Express. The article Manuscript ID is 399831. *No further processing of your paper will occur until we receive your response to this proof.*

Note: *Excessive proof corrections submitted by the author can result in significant delays to publication. Please include only essential changes that might be needed to address any shortcomings noticed in the proof-preparation process.*

Author Queries

Please answer these queries by marking the required corrections at the appropriate point in the text or referring to the relevant line number in your PDF proof.

	No Query

Other Items to Check

- Please note that the original manuscript has been converted to XML prior to the creation of the PDF proof, as described above. The PDF proof was generated using LaTeX for typesetting. The placement of your figures and tables may not be identical to your original paper.
- Please carefully check all key elements of the paper, particularly the equations and tabular data.
- Author list: Please make sure all authors are presented, in the appropriate order, and that all names are spelled correctly.
- If you need to supply new or replacement figures, please place the figures in a Word or LaTeX manuscript template at the desired final figure size. Upload a PDF version of the document with figures when submitting proof corrections.

Optics EXPRESS

Monitoring the aspect ratio distribution of colloidal gold nanoparticles under pulsed-laser exposure

YEHIA MANSOUR, YANN BATTIE,* AOTMANE EN NACIRI, AND NOUARI CHAOUI

Université de Lorraine, LCP-A2MC, F-57000 Metz, France
*yann.battie@univ-lorraine.fr

Abstract: We propose an advanced in situ extinction spectroscopy set up to investigate the dynamic of the fragmentation and reshaping processes of gold colloids during a ns-laser pulse exposure. The evolution of the aspect ratio distribution of gold nanorods (NRs) during the laser exposure is obtained by analyzing each spectra with the shape distributed effective medium theory. We demonstrate that the kinetics of NR shape transformation can be divided into two fluence regimes. At small fluence, the kinetic is limited by the NRs orientation, while at high fluence, the fragmentation rate is only limited by the probability of NRs to be located in the irradiated volume.

© 2020 Optical Society of America under the terms of the OSA Open Access Publishing Agreement

1. Introduction

Metal nanoparticles (NPs) exhibit unique optical properties such as surface plasmon resonances (SPRs) coming from the collective oscillations of their surface conduction electrons. SPR is increasingly used in many fields of applied sciences. The position and amplitude of SPR bands depend on the size, shape and environment of the NPs [1,2]. Frontier areas of research and development require the precise control of the NP size and shape [3,4]. Therefore, the control of the size/shape distributions of the NPs is of great importance for plasmonic devices.

Among the control methods [5,6], pulsed-laser fragmentation and reshaping can be considered as an attractive way to refine the NP shape distribution. Several authors demonstrated the effectiveness of the use of pulsed-lasers to control of the size and aspect ratio distribution of the NPs. Numerous experimental and theoretical investigations of the mechanisms of laser interaction with colloidal NPs have been conducted to have a smart control of the distributions [7–10]. That is why many researches were invested into real time observation of the evolution of NPs during laser exposure by using several techniques such as small angle X-ray scattering (SAXS) [11,12], X-ray absorption fine structure (XAFS) [13,14] or extinction spectrometry [15–18]. In this sense, S. Link *et al.* [19] have studied the shape changes of colloidal gold nanorods (NRs) during exposure to femtosecond and nanosecond laser pulses by recorded an extinction spectra corresponds to an increased number of absorbed laser pulses. A strong correlation between the characteristics of the extinction spectra and the NPs shape evolution was demonstrated after the laser exposure. Similarly, A. Attia *et al.* [20] recorded extinction spectra during ns-pulsed laser irradiation of Au NRs at various wavelengths. M. Barberio *et al.* [21] monitored the size evolution of Au NPs produced by laser ablation in liquid medium using absorption spectrometry and Mie theory. The effective medium theory was also used elsewhere for the investigation of average aspect ratio and volume fraction temporal evolution of the seeded growth processes of gold nanoparticles [22]. Recently an effective medium theory based on a mean field and quasistatic approach was introduced to describe the optical properties of spheroids distributed in aspect ratio [23–27]. This model, named shape distributed effective medium theory (SDEMT), takes into account the NPs aspect ratio distribution. It was used to explain the impact of aspect

#399831 https://doi.org/10.1364/OE.399831
Journal © 0000 Received 9 Jun 2020; revised 21 Jul 2020; accepted 21 Jul 2020; published 00 00 0000

Optics EXPRESS

ratio distribution on the plasmon band of silver and gold NPs [24]. Simulations performed with this model revealed that the dependency of the plasmon band position and width on the mean value and standard deviation of depolarization parameters, respectively [24].

In this paper, the SDEMT model is used to monitor the aspect ratio distribution of Au NPs exposed to ns-laser pulses. Herein, in-situ extinction spectra were recorded in real time during the process. The evolution the aspect ratio distributions of the Au NPs was then determined by fitting each spectra using the SDEMT model. The as-obtained aspect ratio distributions were compared to those obtained by transmission electron microscopy (TEM). In contrast with TEM measurements, the proposed approach has the advantage of being noninvasive and enables the monitoring of NP aspect ratio evolution during laser exposure. Based on the evolution of the aspect ratio distribution, the laser-colloids time constant, which characterizes the kinetic of the evolution of the NP aspect ratio distribution, can be extracted for several fluences and initial distributions. We demonstrate that the evolution of time constant as a function of laser fluence shows two regimes. In the first regime, which occurs at low fluence, it is found that the time constant depends on the initial aspect ratio distribution. In contrast, in the second regime, it becomes independent on the initial aspect ratio distribution. The occurrence of these two regimes is rationalized by a modified Takami model [9], which allows the calculation of the time constant. We show that in the low fluence regime the process is governed by the dependence of the NRs orientation with respect to the ns-laser polarization while in the second one it becomes independent on the NRs orientation.

2. Experimental and theoretical methods

2.1. Experimental methods

Three Au colloidal suspensions named S_1, S_2 and S_3 were investigated. S_2 and S_3 were purchased from Sigma Aldrich while S_1 was made according to the seed-mediated growth method [28]. First, a seed suspension is synthesized by mixing 5 ml of an aqueous solution containing 5×10^{-4} M of $HAuCl_4$ and 0.2 M of CTAB with 0.6 ml of ice-cold 0.01 M $NaBH_4$. Then, S_3 was obtained by mixing 0.25 ml of a solution containing 4×10^{-3} M $AgNO_3$ and 0.2 M CTAB, 70 µl of 0.08 M ascorbic acid, 5.0 ml of 0.001 M $HAuCl_4$ and 12 µl of the seed suspension. The obtained NRs were characterized with a Phillips CM200 TEM operated at 200 kV. The TEM samples were prepared by evaporating a drop of colloidal suspension on a carbon-coated copper grid. The TEM images of the NPs/NRs prior to laser exposure are shown in Fig. 1. S_1 NPs (Fig. 1(a)) exhibits a broad NPs aspect ratio and size distribution. It is observed that S_1 is composed of a mixture of nanorods (NRs) and almost spherical NPs. Their aspect ratio and minimum Feret diameter are in the 0.2-1 and 3-25 nm ranges, respectively. S_2 colloidal suspension (Fig. 1(b)) is composed of NPs with narrow aspect ratio distributions showing mean aspect ratio and minimum Feret diameter of S_2 NRs are 0.6 and 27 nm, respectively. S_3 colloidal suspension contains NRs with mean aspect ratio and minimum Feret diameter of 0.28 and 8 nm, respectively (Fig. 1(c)).

For irradiation experiments, 2 ml of the colloidal suspension was introduced in a 1 cm light-path quartz cell, which is horizontally exposed to ns-laser pulses. The suspension was continuously stirred with a magnetic stirrer during the laser exposure. The laser pulses were delivered from a Nd-YAG laser (Continuum Surelite I) set to its fundamental wavelength (1064 nm). The pulses width and repetition rate were 6 ns and 10 Hz, respectively. The laser energy and fluence was adjusted by varying the Q-switch delay keeping the output laser beam diameter constant (4 mm in diameter). The spatial profile of the output beam was reshaped by means of an intracavity apodizer in order to attenuate the hot spots inherent to the elliptical pumping configuration of the laser rod.

Extinction spectra of the suspensions were recorded *in situ* and during the laser exposure according to the set-up shown in Fig. 2. The UV-visible light emitted from a xenon source was collimated by a set of two quartz lens (f=150 mm) and a slit. The collimated beam was then

Optics EXPRESS

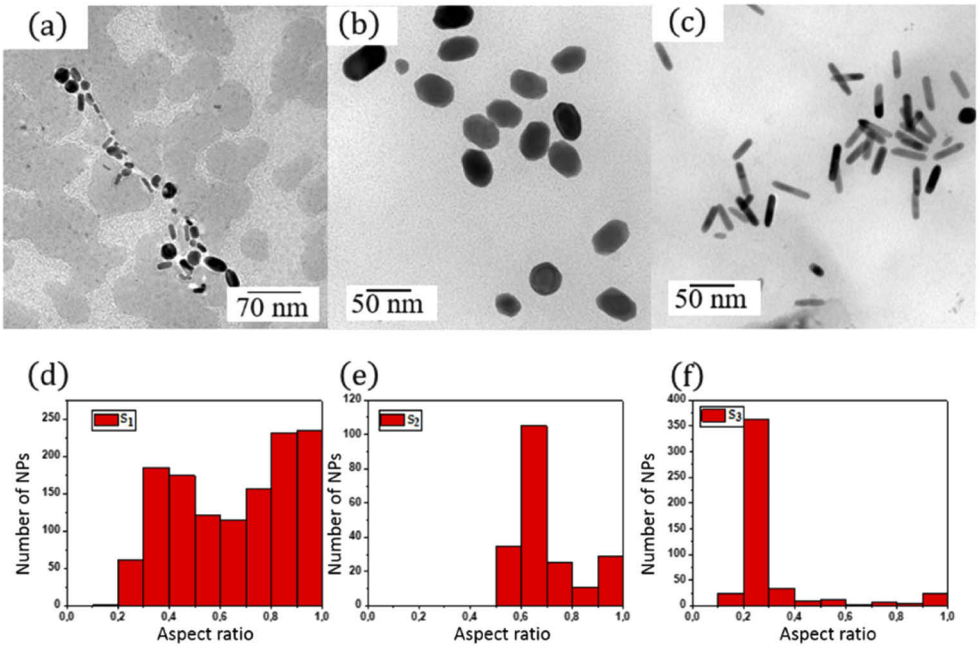

Fig. 1. (a)(b)(c) TEM images and (d)(e)(f) NP aspect ratio distributions of samples (a)(d) S_1, (b)(e) S_2 and (c)(d) S_3.

focused at the center of the quartz cell by means of a 90° off-axis parabolic mirror (f=150 mm) and collimated by a second off-axis parabolic mirror with identical characteristics. It was then sent into an AvaSpec-ULS2048L-USB2 spectrometer (Avantes) via a parabolic collector coupled with an optical fiber. The extinction spectra of the colloidal suspension were recorded in range of 400-900 nm and an acquisition rate of 10 Hz.

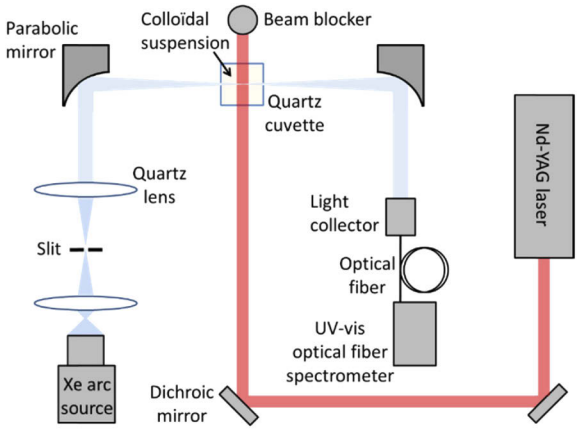

Fig. 2. Schematic diagram of the experimental setup used to record the extinction spectra of the colloidal suspension during pulsed-laser exposure.

Optics EXPRESS

2.2. Shape distributed effective medium theory

The optical properties of metallic nanoparticles (NPs) dispersed in liquid (water) and distributed in aspect ratio are investigated by using the shape distributed effective medium theory (SDEMT) [23–27]. By considering the quasistatic approximation, the spatial average of electric field ($\left\langle \vec{E} \right\rangle$) and displacement field ($\left\langle \vec{D} \right\rangle = \varepsilon_{eff} \left\langle \vec{E} \right\rangle$) in colloidal suspension are the sum of two contributions:

$$\left\langle \vec{E} \right\rangle = (1-f) \left\langle \overrightarrow{E_m} \right\rangle + f \left\langle \overrightarrow{E_{np}} \right\rangle, \tag{1}$$

$$\varepsilon_{eff} \left\langle \vec{E} \right\rangle = (1-f)\varepsilon_m \left\langle \overrightarrow{E_m} \right\rangle + f\varepsilon_{np} \left\langle \overrightarrow{E_{np}} \right\rangle, \tag{2}$$

where f is the volume fraction of NPs. ε_m and ε_{np} are the dielectric function of the water and Au NPs, respectively. They are extracted from the Palik handbook [29]. $\left\langle \overrightarrow{E_{np}} \right\rangle$ and $\left\langle \overrightarrow{E_m} \right\rangle$ are the spatial average electric fields inside the NPs and inside matrix, respectively. These fields are linked together by:

$$\left\langle \overrightarrow{E_{np}} \right\rangle = \langle \lambda \rangle \left\langle \overrightarrow{E_m} \right\rangle. \tag{3}$$

For randomly oriented NRs, The slope $\langle \lambda \rangle$ is given by:

$$\langle \lambda \rangle = \int_0^{1/3} P(L_{1,}) \frac{\varepsilon_m}{3} \left(\frac{1}{\varepsilon_m + L_1(\varepsilon_{np} - \varepsilon_m)} + \frac{2}{\varepsilon_m + 0.5(1-L_1)(\varepsilon_{np} - \varepsilon_m)} \right) dL_1, \tag{4}$$

where L_1 is the depolarization parameter of NRs along their major axis. This parameter only depend on the NP morphology. The NP aspect ratio distribution is taken into account thanks to the distribution of depolarization parameter $P(L_1)$. According to TEM, colloidal suspensions are composed of two populations of NPs: spherical NPs and NRs which can be assimilated to prolate NPs. Thus, we assume that $P(L_1)$ is described by a normalized bi-Gaussian distribution:

$$P(L_1) = N(N_s e^{-\frac{\left(L_1 - \frac{1}{3}\right)^2}{2\sigma_s{}^2}} + e^{-\frac{(L_1 - \overline{L_1})^2}{2\sigma_p{}^2}}). \tag{5}$$

The first and the second terms of Eq. (5) are related to almost spherical NPs and NRs, respectively. $\overline{L_1}$ is the mean values of the depolarization parameters of NRs. σ_s and σ_p are the standard deviation of spherical NPs and NRs aspect ratio distribution, respectively. N is a normalization constant and N_s is a relative ratio between spherical NPs and NRs. The effective dielectric function of a medium composed of NRs distributed in aspect ratio and randomly oriented can be obtained by combining Eqs. (1)–(3) [23–27]:

$$\varepsilon_{eff} = \frac{(1-f)\varepsilon_m + f\varepsilon_{np} \langle \lambda \rangle}{(1-f) + f \langle \lambda \rangle}, \tag{6}$$

The extinction coefficient α of the medium is then calculated from the following equation:

$$\alpha = \frac{4\pi}{\lambda} * Im\left(\sqrt{\varepsilon_{eff}}\right). \tag{7}$$

We must keep in mind that the SDEMT is based on quasistatic approximation. Therefore, the extinction coefficient obtained from the SDEMT model is accurate if the following conditions are fulfilled:

- The NPs size must be negligible compare to the wavelength.
- The scattering cross section must be negligible compared to the absorption cross section of NPs.
- The volume fraction of NPs must be small enough to neglect the interaction between NPs.

Optics EXPRESS

2.3. Modified Takami model (MTM)

According to our previous work [9], the interaction between colloidal gold nanorods (NRs) and ns-laser pulses can be described by the modified Takami model (MTM). Using the energy conservation principle. The MTM model simulates the evolution of the nanoparticle temperature by using the following set of equations:

$$\rho_s \frac{\pi d^3}{12}\left(\frac{3}{r}-1\right) C_s \frac{dT}{dt} + \pi d\kappa(T-T_0) + \delta \frac{\pi d^2}{r} T^4 - \sigma\, F_0 e^{-\alpha Z} e^{-0.5\left(\frac{t-t_p}{\tau_L}\right)^2} = 0 \; for\; T<T_m, \quad (8)$$

$$\rho_s \frac{\pi d^3}{12}\left(\frac{3}{r}-1\right) \Delta H_m + \int_{t_1}^{t_1+t_m} \pi d\kappa(T_m-T_0) + \delta \frac{\pi d^2}{r} T_m^4 - \sigma\, F_0 e^{-\alpha Z} e^{-0.5\left(\frac{t-t_p}{\tau_L}\right)^2} dt = 0 \; for\; T = T_m\,, \quad (9)$$

$$\rho_l \frac{\pi d^3}{12}\left(\frac{3}{r}-1\right) C_l \frac{dT}{dt} + \pi d\kappa(T-T_0) + \delta \frac{\pi d^2}{r} T^4 - \sigma\, F_0 e^{-\alpha Z} e^{-0.5\left(\frac{t-t_p}{\tau_L}\right)^2} = 0 \; for\; T_m<T<T_b, \quad (10)$$

$$\rho_l \frac{\pi d^3}{12}\left(\frac{3}{r}-1\right) \Delta H_b + \int_{t_2}^{t_2+t_b} \pi d\kappa(T_b-T_0) + \delta \frac{\pi d^2}{r} T_b^4 - \sigma\, F_0 e^{-\alpha Z} e^{-0.5\left(\frac{t-t_p}{\tau_L}\right)^2} dt = 0 \; for\; T = T_b. \quad (11)$$

The first term of Eqs. (8)–(11) represents the heat of NR while the second and the third terms denote the conductive and the radiative losses, respectively. The last term of Eqs. (8)–(11) describes the absorbed light energy by considering a Gaussian ns-pulse centered at t_p=6 ns with a standard deviation τ_L=2 ns. F_0 is the maximum fluence value of the pulse while α and Z are the extinction coefficient of the colloidal suspension measured at 1064 nm and the position of the NRs along the laser beam in the cell, respectively. ρ_s = 19.32 g.cm^{-3} and C_s = 0.129 J.g^{-1}.K^{-1} are the density and the heat capacity of Au in the solid state, respectively. ρ_l = 17.31 g.cm^{-3} and C_l = 0.15 J.g^{-1}.K^{-1} are the density and the heat capacity of Au in the liquid state, respectively. r and d are the aspect ratio and the minimum Feret diameter of NRs, respectively. T_0=298 K is the temperature of the solvent. δ = 5.67 10^{-8} W.m^{-2}.K^{-4} is the Stefan-Boltzmann constant, respectively. Due to the release of energy from NP to its environment, a thin layer of water vapor is assumed to be formed around the NP [30]. This layer is assumed to act as a thermal shield, which limits the dissipation of energy by convective losses. To take into account this effect, we use the thermal conductivity water vapor κ=0.0239 W.m^{-1}.K^{-1}. As SDEMT model describes the optical properties of a collection of NRs distributed in aspect ratio, this model cannot be used to determine the absorption cross section of individual NR. In addition, due to the NPs aspect ratio distribution in colloidal suspensions, we cannot determine the absorption cross section of individual NRs from absorption spectroscopy measurements. Thus, the absorption cross section σ of individual Au NR in water is evaluated at 1064 nm (laser wavelength) by using the boundary element method. According to its symmetry, Au NRs support two plasmon resonances: the transversal (T-SPR) and the longitudinal plasmon modes (L-SPR) which can be selectively excited with a light polarized along the minor and major axes of NRs, respectively. Thus, we calculate the absorption cross section (σ_{L-SPR}, σ_{T-SPR}) for these two eigen polarization states. Then, the absorption cross section $\sigma(\theta,\varphi)$ for any NR orientations is deduced from the following equation:

$$\sigma(\theta,\varphi) = \sigma_{L-SPR}\; sin^2(\varphi)cos^2(\theta) + \sigma_{T-SPR}\; (sin^2(\varphi)sin^2(\theta) + cos^2(\varphi)). \quad (12)$$

The angles θ and φ give the orientation of NR with respect to the incident polarization. Depending on the laser fluence and the absorption cross section, the temperature rise of the NRs during the laser pulse, results in phase transitions, which determine the shape of the NRs after laser exposure:

- The NRs is unmodified if $T \leq T_m$ and $t \leq t_1$.

Optics EXPRESS

- The NRs is partially melted and reshaped in surface if $T = T_m$ and $t_1 \leq t \leq t_1 + t_m$.
- The NRs is completely melted and reshaped into spherical NP if $T_m \leq T \leq T_b$ and $t_1 + t_m \leq t \leq t_2$.
- The NRs is partially vaporized and fragmented if $T = T_b$ and $t_2 \leq t \leq t_2 + t_b$. The partial fragmentation produces clusters and a spherical NP.

The NRs is completely vaporized and fragmented if $T_b \leq T$ and $t_2 + t_b \leq t$. The fragmentation produces clusters

As we have shown previously, the MTM model can be used to estimate the shape distribution of NPs after their exposure to ns-laser pulses [9].

3. Results and discussion

3.1. Effect of the NPs distribution

In order to study the effect of the initial aspect ratio distribution on the shape evolution of the NPs and NRs, three different gold colloidal suspensions S_1, S_2 and S_3 were exposed to laser pulses at a fluence of 0.8 J.cm^{-2}. Figures 3(a), (b), and (c) shows the in-situ extinction spectra as a function of pulse number. Prior to laser exposure, the optical spectra (Fig. 8 in Appendix A) show the presence for each sample of two bands, centered at 730 nm and 530 nm for S_1, at 560 nm and 526 nm for S_2, and at 830 nm and 509 nm for S_3. The first band is attributed to the longitudinal plasmon resonance of the NRs, and the second one to a convolution of the transversal plasmon of the NRs and the plasmon band of the spherical NPs. The amplitude of the longitudinal plasmon bands S_1 and S_3 is found to decrease in favor of the plasmon band of the spherical NPs. However, the absorption spectra of S_2 show that the position and amplitude of the plasmon resonance bands remain constant during the laser irradiation. This can be explained by the fact that the Au NRs in S_1 and S_3 colloidal suspensions transform into spherical NPs during the laser irradiation, while the aspect ratio of the NPs in S_2 suspension remain unchanged.

As the NPs have a sufficiently small size to neglect scattering effect, the measured spectra were then analyzed using the SDEMT model given in the Modeling section. In addition, the Levenberg-Marquardt algorithm was used to solve the inverse problem by minimizing the root mean square error between the measurements and the calculated absorption data. The fit for each spectrum was performed by considering 5 uncorrelated free parameters: the volume fractions f of NPs, the relative ratio between spherical NPs and NRs N_s, the mean value $\overline{L_1}$, and the standard deviations (σ_p, σ_s) of the distribution of depolarization parameters. As unambiguously demonstrated in our previous work [24], the plasmon resonance energies mainly depend on the mean value of the depolarization parameter while the width of the plasmon bands is directly correlated to the standard deviation of the NPs aspect ratio distribution. Therefore, by fitting extinction measurements with SDEMT model, the distribution of depolarization parameter of colloidal gold suspension can be determined and it closely linked to the aspect ratio distribution. Indeed, the depolarization factors of NRs are directly related to their aspect ratio r:

$$L_1 = \frac{r^2}{1-r^2}\left(-1 + \frac{1}{2\sqrt{1-r^2}} \ln\left(\frac{1+\sqrt{1-r^2}}{1-\sqrt{1-r^2}}\right)\right), \tag{13}$$

The calculated spectra from the SDEMT model (Figs. 3(d), (e), and (f) and Fig. 8 in Appendix A) are in agreement with the in situ measured spectra (Figs. 3(a), (b), and (c)). The calculated values of energies, widths and amplitudes of the plasmon bands are close to the experimental values. The model also predicts a decrease of the amplitude of the longitudinal plasmon band of S_1 and S_3 NRs. Moreover, the total volume fraction (f) of NPs remains constant during the fragmentation. The volume fraction of S_1, S_2 and S_3 estimated from the SDEMT model are 3

Optics EXPRESS

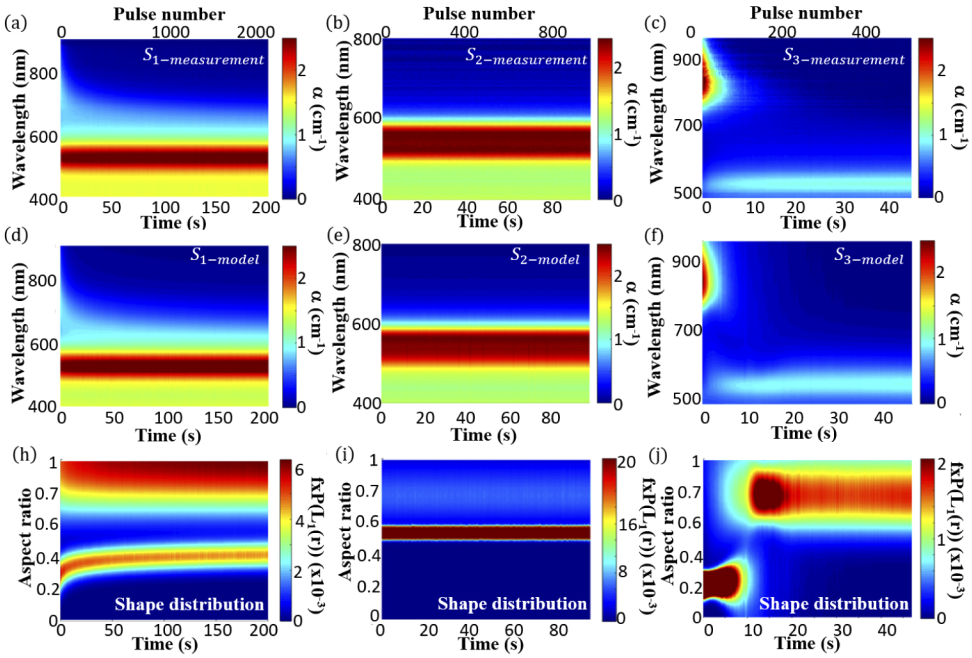

Fig. 3. Time evolution of the extinction spectra measured from the colloidal suspensions (a) S_1, (b) S_2 and (c) S_3 during laser exposure at a 0.8 J.cm^{-2} fluence. Time evolution of the extinction spectra calculated by SDEMT model for the same suspensions (d) S_1, (e) S_2 and (f) S_3. Time evolution of the aspect ratio distribution determined for the suspensions (g) S_1, (h) S_2 and (k) S_3.

ppmv, 2.7 ppmv and 1 ppmv, respectively. The aspect ratio distribution of Au NPs as a function of the laser irradiation time have also been calculated and are shown in Figs. 3(g), (h), and (k). Contrary to several works [31], which limits their analyses to the longitudinal plasmon band of NRs, the modeling of spectra in a large spectral range avoids correlation between free parameters and gives more accurate results in the case of bimodal distribution composed of NRs and nearly spherical NPs. In addition, contrary to several numerical approaches such as boundary element method [32] or discrete dipole approximation [33], the SDEMT requires few computing resources. The accuracy on the distribution depends on the aspect ratio of NR. For nearly spherical NPs, the relative error on the aspect ratio is estimated to 7%. This value decreases with the aspect ratio. Indeed, the relative error is smaller than 1% for an aspect ratio smaller than 0.7.

It is observed that the aspect ratio distribution of S_1 and S_3 change during the laser exposure. A photothermal model based on a modified Takami model (MTM) can predict the mechanisms behind such transformations. We recently introduced this model to explain the mechanisms of shape changes of Au NRs in colloidal suspension induced by ns-laser pulses. This model takes into account the orientation of NRs with respect to the laser polarization, the radiative and convective losses, and the phase transitions of NRs [9].

Based on MTM, the increase of the concentration of spherical NPs in S_1 and S_3 can be attributed to the fragmentation or the complete reshaping of NP. The fragmentation process generates smaller and spherical Au NPs, while the reshaping process is revealed by an increase of the NRs aspect ratio. Therefore, the increase of the NRs aspect ratio in S_1 (Fig. 3(g)) can be related to the reshaping process in which the NRs are melted and cooled before being transformed into spherical NPs due to the surface tension of the molten phase. For S1 suspension, this process is more often observed for NRs having large anisotropy [7,9]. In the case of S_2 suspension, the

Optics EXPRESS

aspect ratio remains unchanged during the irradiation. Indeed, according to the phase diagram simulated with MTM model and shown in Appendix B, most of the NRs are localized between the locus of partial and complete reshaping (Fig. 9 in Appendix B). Therefore, the shape of a large amount of NRs remains unchanged during the laser exposure.

The TEM images of the NPs after laser exposure are reported in Fig. 4. The observed morphology is in agreement with the calculated aspect ratio distribution shown in Fig. 3. As can be seen from Fig. 4(a), sample S_1 after laser exposure (10 min) is composed of smaller spherical Au NPs and NRs which exhibit broad aspect ratio and size distributions. Their average value of their aspect ratio and minimum Feret diameter estimated over more than 1000 NPs are 0.83 and 5.6 nm, respectively. After laser exposure, most of the NRs in sample S_2 remain unchanged (Fig. 4(b)). S_3 is composed of nearly spherical NPs which have an average minimum Feret diameter below 10 nm. Therefore, the NPs aspect ratio observed by TEM after laser exposure is in agreement with the aspect ratio distributions obtained from the SDEMT model (Figs. 3(g), (h), and (k)). Contrary to TEM measurements, the exploitation of extinction spectra with the SDEMT has the advantage of providing *in situ* information about the NPs aspect ratio distribution of colloidal suspension as shown in Fig. 3.

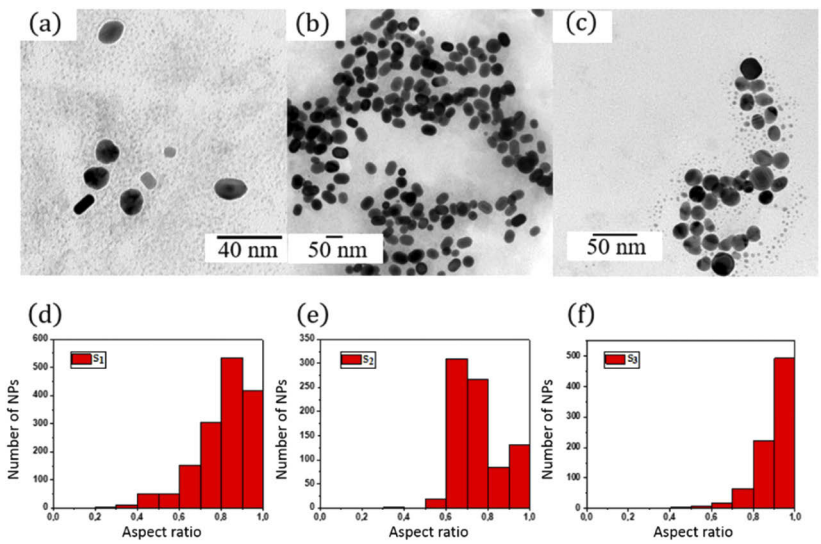

Fig. 4. (a)(b)(c) TEM images of (a) S_1, (b) S_2, (c) S_3 gold NPs after laser exposure, (d)(e)(f) aspect ratio distributions measured by the TEM of (d) S_1, (e) S_2, (f) S_3.

In summary, according to the Fig. 3, we conclude that the evolution of the NPs morphology and their final aspect ratio distribution after laser exposure are affected by their initial aspect ratio distribution.

3.2. Effect of the laser fluence

In our previous work, we have also shown the effect of the laser fluence on the morphology of NPs after exposure to laser pulses [9]. Here, this effect on NPs aspect ratio distribution is investigated as a function of duration of exposure to pulsed-laser i.e., pulses number. To this end, the sample S_3 was exposed to laser pulses at various laser fluences i.e., 3.2 J.cm^{-2}, 1.6 J.cm^{-2} and 0.4 J.cm^{-2}. For sake of clarity, the obtained samples are named S_{3_F}, where F is the laser fluence.

Figure 5 shows the evolution of the aspect ratio of NPs distribution for different laser fluences. A decrease of the concentration of the initial population of NRs is measured at the beginning of each laser exposure. However, due to the range of color scale, these variations do not clearly appear

Optics EXPRESS

in Fig. 5. However, these variations are clearly shown in Fig. 6. At low fluence (Fig. 5(a)), the initial population of the NPs is progressively transformed into a bimodal distribution, composed of almost spherical NPs (aspect ratio close to 1) and NRs with aspect ratios between 0.3 and 0.8, larger than that of the initial one. This result is confirmed by the TEM images of the sample after laser exposure, which is mainly composed of spherical and φ-shape NPs. According to the MTM model, ϕ-shape NPs result from a competition between the reshaping and the cooling process. Indeed, $S_{3_0.4}$ NPs are localized in the locus of reshaping where the laser absorption leads to a complete melting of NPs (Fig. 10 in Appendix B). The molten NPs take a spherical shape to minimize their surface energy. However, due to the finite duration of the process most of NPs are solidified before achieving the spherical shape.

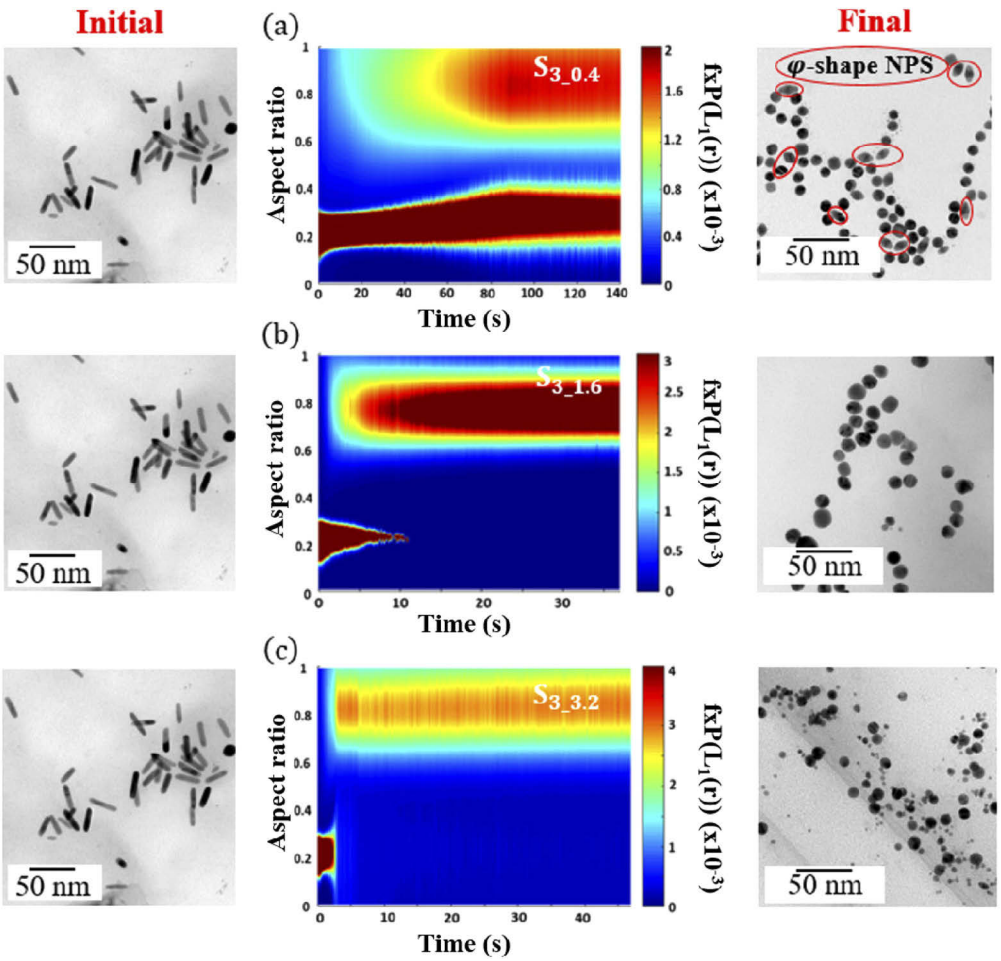

Fig. 5. Aspect ratio distribution as a function of exposure time to laser pulses of the S_3 suspension at various fluences (a) 0.4 J.cm^{-2}, (b) 1.6 J.cm^{-2} and (c) 3.2 J.cm^{-2}; TEM images (left) of initial S_3 NPs, TEM images (right) of S_3 NPs after laser exposure.

The modeling results obtained at intermediate (Fig. 5(b)) and high (Fig. 5(c)) laser fluences are also provided in Fig. 5. Similar final aspect ratio distributions are obtained at 1.6 J.cm^{-2} and at 3.2 J.cm^{-2}. Both samples are composed of nearly spherical NPs after laser exposure, which can be attributed to the partial or complete fragmentation process. Indeed, according to MTM model, the initial NRs distribution is located in the locus of the partial or complete

Optics EXPRESS

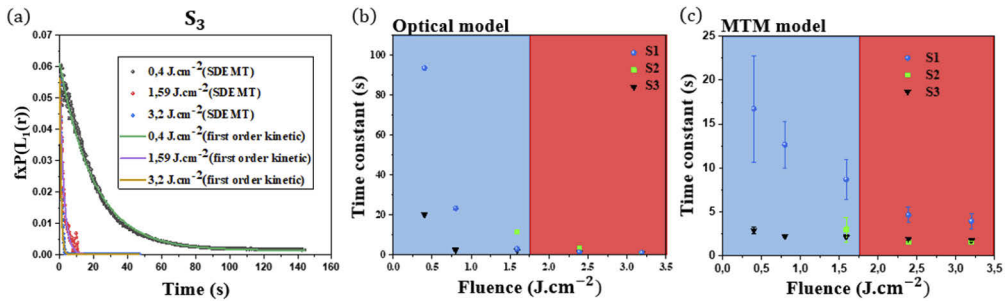

Fig. 6. (a) Evolution of the volume fraction of the NRs with aspect ratio of 0.22 for the suspension S_3 at three different laser fluences, (b) variation of reaction rate as a function of the fluence calculated by fitting the measured volume fraction for different suspensions S_1, S_2 and S_3, (c) variation of the reaction rate as a function of the fluence calculated by the MTM model.

fragmentation, which lead to the formation of small spherical NPs. On the other hand, the NRs surface is evaporated during the partial fragmentation, while their core remain in the liquid state. Therefore, the core of the NRs core is transformed into the more thermodynamically favored spherical shape. Here again, a good agreement is obtained between TEM images showing nearly spherical NPs distribution after laser exposure and the calculated aspect ratio distributions shown in Fig. 5.

3.3. Kinetics of colloidal suspension evolution

The previously described results show that in situ extinction spectroscopy can be used to investigate the kinetics of laser-induced modifications of colloidal suspensions. In the following, we monitor the time-evolution of the volume fraction of NRs with initial mean aspect ratios r_0 of 0.28, 0.54, and 0.22 for samples S_1, S_2, and S_3, respectively. As an example, the modification kinetics of the NRs aspect ratio of sample S_3 is given in Fig. 6(a) for three different laser fluences. The volume fraction of the selected population of NRs is plotted versus exposure duration to lasers pulses. As shown by Fig. 6(a), all these evolutions exhibit an exponential decrease. As illustrated in Fig. 6(a), this variation, attributed to reshaping and fragmentation processes, can be described by a pseudo first-order kinetic law:

$$fP(r_0, t) = ae^{-\frac{t}{\tau}} + b, \tag{14}$$

where r_0 is the selected aspect ratio of NRs. $a + b$ is the volume fraction of NRs at t=0 and b is the remaining volume fraction of NRs with aspect ratio r_0 after laser exposure. Their values were directly estimated from the extinction spectra recorded at the initial and final states. The time constant τ, which is the inverse of the reaction rate, is obtained by using a Levenberg Marquardt fitting procedure. This latter is reported in Fig. 6(b) for several initial distributions and laser fluences. As expected, the time constant decreases by increasing the laser fluences. Two regimes are observed: for fluence below 2 J.cm^{-2}, the reaction rate strongly depends on the initial distribution of NRs and above 2 J.cm^{-2}, the reaction rate becomes independent on the initial aspect ratio distribution.

We applied the MTM model (Eqs. (8)–(11)) to elucidate the mechanism behind these regimes and simulate the evolution of the aspect ratio of 1000 NPs observed by TEM. Each simulation step was associated to the exposure to a subsequent pulse. In addition, it is assumed that after each laser pulse, the NRs cool down to the room temperature. Indeed, this cooling process occurs within at most few µs which is much less than the time between two consecutive pulses (0.1 s). The simulations were conducted on the basis of the following assumptions:

Optics EXPRESS

- The Z position (Fig. 7) of each NP in the cell was randomly chosen in the 0-1 cm range according a uniform distribution. Simulations show that the NRs position in the cell has a negligible impact on the reaction rate. Indeed, due to the low particles concentration and their small absorption cross section at the laser wavelength, the suspensions have a small absorption coefficient at the laser wavelength.

- At each pulse, each NP has a probability P=1/16 to be exposed. This value is defined by the ratio between the irradiated volume and the volume of the colloidal suspensions.

- The NPs are randomly oriented with respect to the beam laser polarization (Fig. 7). Thus, a couple of NPs orientation angles (θ, φ) were randomly chosen for each pulse and each NP.

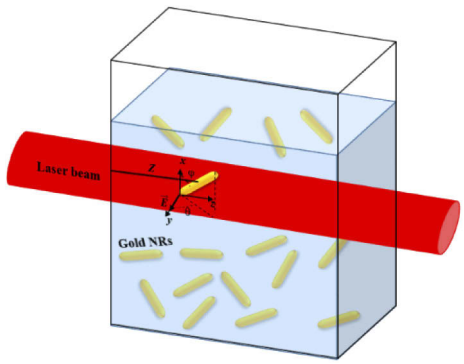

Fig. 7. Schematic diagram of the system considered in simulations: only a small amount of NRs is exposed to the laser beam at each pulse. Each NR has a random orientation defined by the angles (θ, φ) and has a random position Z along the beam path.

It should be noted that a quantitative determination of the reaction time constant is beyond the scope of this simulation. Instead, this simulation qualitatively describes the variation of the reaction rate as a function of laser fluence. The reaction rate is evaluated from the evolution of number of NPs which remain in the $r_0 - 0.1$-$r_0 + 0.1$ range after each calculation step. The simulation results are plotted in Fig. 6(c). In spite of the assumptions made, the model is predictive enough, to reveal the previously observed two fluence regimes in Fig. 6(b). In the first regime, it is found that the reaction rate depends on the NRs orientation and the probability of that the NRs is located in the irradiated volume. Indeed, one should keep in minds that according to Eq. (12), the absorption cross section of a NR depends on its orientation relative to the direction of laser polarization. At the laser wavelength, it reaches a maximum value when the longitudinal plasmon mode of NRs is selectively exited. In other words, only the NRs which are oriented close to the laser polarization can be reshaped or fragmented. Thus, the NRs must be exposed to several pulses before undergoing an aspect ratio modification. In the high fluence regime, the absorbed energy is sufficiently high to induce a phase transition whatever the NR orientation. In this case, the reaction rate is mainly governed by the probability of a NR to be located in the irradiated volume and this probability does not dependent on the initial aspect ratio distribution. This result explains why all the reaction time constants tend towards the same value at high fluence.

4. Conclusion

In summary, we have developed an in situ extinction spectroscopy set up to investigate the dynamic of the fragmentation and reshaping processes of Au NPs induced ns-laser pulses. Each

Optics EXPRESS

recorded spectra is analyzed with the SDEMT model. We show that the modeled spectra by the SDEMT are close to the measured ones. In addition, the aspect ratio distributions of NPs estimated from the SDEMT before and after the laser exposure are in agreement with those determined by TEM. Contrary to TEM, our technic allows determining the evolution of the NRs aspect ratio distribution along the exposure to laser pulses. We show that the evolution of the NRs aspect ratio can be satisfactorily described by a first order kinetic law which reaction rate decreases with laser fluence. Using the MTM model, we demonstrate that the kinetics of NRs aspect ratio transformation can be divided into two fluence regimes: a low regime for which the kinetic is mainly limited by the orientation of NPs and a high fluence regime in which the reaction rate is independent on the initial shape distribution of the NRs and is only limited by the probability of NRs to be located in the irradiated volume.

Appendix A: initial extinction spectra of S_1, S_2 and S_3

Figure 8 shows the measured and calculated initial extinction spectra of S_1, S_2 and S_3.

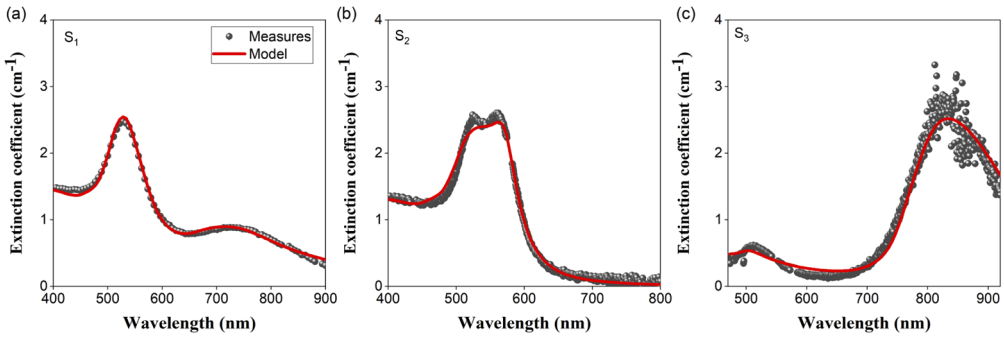

Fig. 8. The measured and calculated initial extinction spectra of S_1, S_2 and S_3.

Appendix B: metastable phase diagram

Figure 9 shows the metastable phase diagram simulated with the Modified Takami Model (MTM) for a laser fluence of 0.8 J.cm^{-2}. The initial and final distributions of S_1, S_2 and S_3 NPs, obtained by TEM, are also reported. The metastable phase diagram predicts the shape transformation between the initial and the final distribution.

Each NP observed by TEM before and after the laser exposure, is reported in the metastable phase diagrams (Fig. 9). Part of initial NPs for S_1 and S_3 is localized in the complete or partial fragmentation domains, suggesting the formation of spherical nanoparticles. The other part of initial NPs for S_1 and S_2 is localized in the complete and partial reshaping domains. Due to the cooling process of the NP induced by the heat losses, the NPs are solidified before reaching the spherical shape. These phenomena induces the formation of the NP with an aspect ratio larger than the initial NP.

Figure 10 shows the comparison between the phase diagrams of Au NRs simulated from the MTM model for 3 laser fluences: 0.4, 1.6 and 3.2 J.cm^{-2}. The initial and final distributions of $S_{3_0.4}$, $S_{3_1.6}$, $S_{3_3.2}$ NPs, obtained by TEM are also reported.

At these fluences, part of nanoparticles is localized in the total fragmentation domain suggesting that the laser exposure induces the formation of spherical nanoparticles. This result explains the increase of the concentration of spherical nanoparticles during the laser exposure. The other part of $S_{3_0.4}$ NPs is localized in the partial fragmentation and the total reshaping domains, suggesting the formation of NP with a larger aspect ratio. This result explains the increase of the average aspect ratio of the NRs during the laser exposure.

Optics EXPRESS

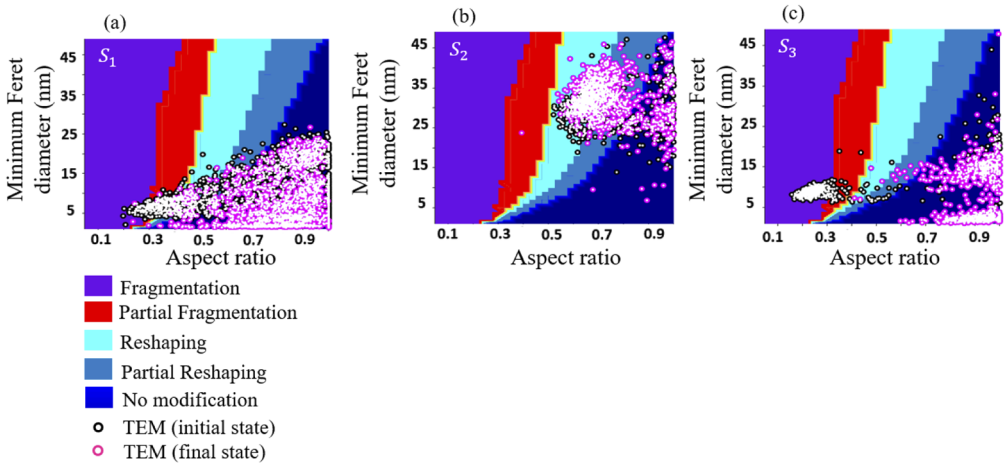

Fig. 9. Metastable phase diagrams in the space of Au NRs calculated at 0.8 J.cm^{-2} laser fluences. Each (a) S_1 (b) S_2, (c) S_3 NP observed by TEM after the laser exposure is represented as a pink dot. The raw NPs observed in (a) S_1, (b) S_2 and (c) S_3 are represented by black dots.

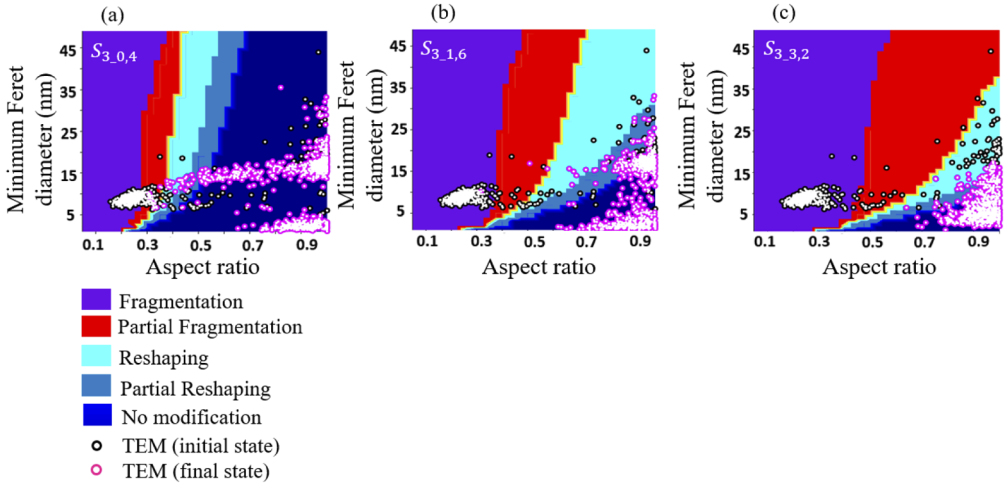

Fig. 10. Metastable phase diagrams in the space of Au NRs calculated at (a) 0.4, (b) 1.6 and (c) 3.2 J.cm^{-2} laser fluences. Each a) $S_{3_0.4}$ (b) $S_{3_1.6}$, (c) $S_{3_3.2}$ NP observed by TEM after laser exposure is represented as a pink dot. The raw NPs observed in (a) $S_{3_0.4}$ (b) $S_{3_1.6}$, (c) $S_{3_3.2}$ before laser exposure are also represented by black dots.

Optics EXPRESS

Disclosures

The authors declare no conflicts of interest.

References

1. K.-S. Lee and M. A. El-Sayed, "Gold and silver nanoparticles in sensing and imaging: sensitivity of plasmon response to size, shape, and metal composition," J. Phys. Chem. B **110**(39), 19220–19225 (2006).
2. M. M. Miller and A. A. Lazarides, "Sensitivity of metal nanoparticle surface plasmon resonance to the dielectric environment," J. Phys. Chem. B **109**(46), 21556–21565 (2005).
3. A. D. McFarland and R. P. Van Duyne, "Single silver nanoparticles as real-time optical sensors with zeptomole sensitivity," Nano Lett. **3**(8), 1057–1062 (2003).
4. K. R. Catchpole and A. Polman, "Plasmonic solar cells," Opt. Express **16**(26), 21793–21800 (2008).
5. G.-T. Wei, F. K. Liu, and C. R. C. Wang, "Shape separation of nanometer gold particles by size-exclusion chromatography," Anal. Chem. **71**(11), 2085–2091 (1999).
6. R. Omar, A. En Naciri, S. Jradi, Y. Battie, J. Toufaily, H. Mortadab, and S. Akil, "One-step synthesis of a monolayer of monodisperse gold nanocubes for SERS substrates," J. Mater. Chem. C **5**(41), 10813–10821 (2017).
7. S. Link, L. Z. Wang, and M. A. El-Sayed, "How does a gold nanorod melt?" J. Phys. Chem. B **104**(33), 7867–7870 (2000).
8. A. Takami, H. Kurita, and S. Koda, "Laser-induced size reduction of noble metal particles," J. Phys. Chem. B **103**(8), 1226–1232 (1999).
9. Y. Mansour, Y. Battie, A. En Naciri, and N. Chaoui, "Mechanisms and advanced photothermal modelling of laser-induced shape transformations of colloidal gold nanorods by nanosecond laser pulses," Nanoscale **11**(24), 11679–11686 (2019).
10. A. Pyatenko, H. Wang, N. Koshizaki, and T. Tsuji, "Mechanism of pulse laser interaction with colloidal nanoparticles," Laser Photonics Rev. **7**(4), 596–604 (2013).
11. M. Harada, N. Tamura, and M. Takenaka, "Nucleation and growth of metal nanoparticles during photoreduction using in-situ time-resolved SAXS analysis," J. Phys. Chem. C **115**(29), 14081–14092 (2011).
12. J. A. Balmer, O. O. Mykhaylyk, S. P. Armes, J. P. A. Fairclough, A. J. Ryan, J. Gummel, M. W. Murray, K. A. Murray, and N. S. J. Williams, "Time-resolved small-angle X-ray scattering studies of polymer-silica nanocomposite particles: initial formation and subsequent silica redistribution," J. Am. Chem. Soc. **133**(4), 826–837 (2011).
13. Z. H. Sun, H. Oyanagi, M. Uehara, H. Nakamura, K. Yamashita, A. Fukano, and H. Maeda, "Study on initial kinetics of CdSe nanocrystals by a combination of in-situ X-ray absorption fine structure and microfluidic reactor," J. Phys. Chem. C **113**(43), 18608–18613 (2009).
14. M. Harada, Y. Inada, and M. Nomura, "In-situ time resolved XAFS analysis of silver particles formation by photoreduction in polymer solutions," J. Colloid Interface Sci. **337**(2), 427–438 (2009).
15. T. Nakamura, Y. Herbani, D. Ursescu, R. Banici, R. V. Dabu, and S. Sato, "Spectroscopic study of gold nanoparticle formation through high intensity laser irradiation of solution," AIP Adv. **3**(8), 082101 (2013)..
16. D. Werner, S. Hashimoto, T. Tomita, S. Matsuo, and Y. Makita, "In-situ spectroscopic measurements of laser ablation-induced splitting and agglomeration of metal nanoparticles in solution," J. Phys. Chem. C **112**(43), 16801–16808 (2008).
17. M. Gordel, J. Olesiak-Banska, K. Matczyszyn, C. Nogues, M. Buckleb, and M. Samoca, "Post-synthesis reshaping of gold nanorods using a femtosecond laser," Phys. Chem. Chem. Phys. **16**(1), 71–78 (2014).
18. S. Wei and K.-I. Saitow, "In-situ multipurpose time-resolved spectrometer for monitoring nanoparticle generation in a high pressure fluid," Rev. Sci. Instrum. **83**(7), 073110 (2012)..
19. S. Link, C. Burda, B. Nikoobakht, and M. A. El-Sayed, "Laser-induced shape changes of colloidal gold nanorods using femtosecond and nanosecond laser pulses," J. Phys. Chem. B **104**(26), 6152–6163 (2000).
20. Y. A. Attia, M. T. Flores-Arias, D. Nieto, C. Vázquez-Vázquez, G. F. De La Fuente, and M. A. López-Quintela, "Transformation of gold nanorods in liquid media induced by NIR, visible, and UV laser irradiation," J. Phys. Chem. C **119**(23), 13343–13349 (2015).
21. M. Barberio and P. Antici, "In-situ study of nucleation and aggregation phases for nanoparticles grown by laser-driven methods," Sci. Rep. **7**(1), 41372–41380 (2017).
22. M. R. Andalibi, A. Wokaun, P. Bowen, and A. Testino, "Kinetics and mechanism of metal nanoparticle growth via optical extinction spectroscopy and computational modeling: The curious case of colloidal gold," ACS Nano **13**(10), 11510–11521 (2019).
23. Y. Battie, A. En Naciri, W. Chamorro, and D. Horwat, "Generalized effective medium theory to extract the optical properties of two-dimensional nonspherical metallic nanoparticle layers," J. Phys. Chem. C **118**(9), 4899–4905 (2014).
24. A. Resano-Garcia, Y. Battie, A. En Naciri, S. Akil, and N. Chaoui, "Experimental and theoretical determination of plasmonic responses and shape distribution of colloidal metallic nanoparticles," J. Chem. Phys. **142**(13), 134108–134117 (2015).
25. Y. Battie, A. Resano-Garcia, A. En Naciri, S. Akil, and N. Chaoui, "Determination of morphological characteristics of metallic nanoparticles based on modified Maxwell-Garnett fitting of optical responses," Appl. Phys. Lett. **107**(14), 143104 (2015)..

Optics EXPRESS

26. Y. Battie, I. Izquierdo-Lorenzo, A. Resano-Garcia, A. En Naciri, S. Akil, P. M. Adam, and S. Jradi, "How to determine the morphology of plasmonic nanocrystals without transmission electron microscopy?" J. Nanopart. Res. **18**(8), 217 (2016)..
27. Y. Battie and A. En Naciri, "Roadmap of ellipsometric characterization of plasmonic nanoparticle," J. Vac. Sci. Technol., B: Nanotechnol. Microelectron.: Mater., Process., Meas., Phenom. **37**(6), 062912 (2019)..
28. B. Nikoobakht and M. A. El-Sayed, "Preparation and growth mechanism of gold nanorods (NRs) using seed-mediated growth method," Chem. Mater. **15**(10), 1957–1962 (2003).
29. E. D. Palik, *Handbook of optical constants of solids*, Academic, 1998.
30. D. Lapotko, "Optical excitation and detection of vapor bubbles around plasmonic nanoparticles," Opt. Express **17**(4), 2538–2556 (2009).
31. S. Eustis and M. A. El-Sayed, "Determination of the aspect ratio statistical distribution of gold nanorods in solution from a theoretical fit of the observed inhomogeneously broadened longitudinal plasmon resonance absorption spectrum," J. Appl. Phys. **100**(4), 044324 (2006)..
32. U. Hohenester and A. Trügler, "MNPBEM–A Matlab toolbox for the simulation of plasmonic nanoparticles," Comput. Phys. Commun. **183**(2), 370–381 (2012).
33. B. T. Draine and P. J. Flatau, "Discrete dipole approximation for scattering calculations," J. Opt. Soc. Am. A **11**(4), 1491–1499 (1994).